Plasmonic concentrator of magnetic field of light

Piotr Wróbel,[1,a)] Tomasz J. Antosiewicz,[2,a)] Tomasz Stefaniuk,[1] and Tomasz Szoplik[1,b)]

[1)] *University of Warsaw, Faculty of Physics, Pasteura 7, 02-093 Warsaw, Poland*

[2)] *Chalmers University of Technology, Department of Applied Physics, SE-412 96 Göteborg, Sweden*

(Dated: 21 August 2012)

We propose an efficient concentrator of the magnetic component of evanescent field of light for measuring magnetic responses of nanostructures. It is in the form of a tapered fiber probe, which in its final part has corrugations along the angular dimension and is coated with metal except for the aperture at the tip. Internal, azimuthally polarized illumination is concentrated into a subwavelength spot with a strong longitudinal magnetic component H_z. Within the visual range of wavelengths 400-700 nm the energy density of H_z is up to 50 times larger than that of the azimuthal electric E_ϕ one. This dominant H_z contribution may be used for magnetic excitation of elementary cells of metamaterials with a single probe guiding a wide spectrum of generated plasmons.

PACS numbers: 75.75.-c, 73.20.Mf, 68.37.Uv, 78.67.Pt

[a)] These authors contributed equally.

[b)] Electronic mail: tszoplik@mimuw.edu.pl

I. INTRODUCTION

Artificial materials with non-unity magnetic permeability μ at high frequencies attract a lot of attention because of their potential use in invisibility cloaking. Magnetic metamaterials were first proposed in the form of 2D and 3D structures composed of split ring resonators (SRRs).[1] In early designs, resonant frequencies were observed in the $5 \div 15$ GHz range, where $\mathrm{Im}(\mu)$ was always positive and grew from virtually zero level to a value of a few.[2–6] In the vicinity of the resonances of effective permeability anomalous dispersion with decreasing $\mathrm{Re}(\mu)$ values were observed. In the last decade metamaterials with strong magnetic response and a negative imaginary part of permeability was minimized from millimeter-sized unit cells[7,8] to nanometer-sized[9] to achieve a magnetic response in the visible blue range.[10] In 2009 Merlin assessed that non-unity permeability is achievable in metamaterials composed of dielectrics with large permittivity.[11] Thus, a need for methods to measure the magnetic response of elementary cells of magnetic metamaterials has appeared.

The first means to measure the magnetic field of light locally appeared more than a decade ago. Using a scanning near-field optical microscope (SNOM) in the inverse transmission mode Devaux *et al.*[12] observed that a tapered gold-coated probe collects a signal proportional to the square modulus of the magnetic component of the optical near field. Investigation of magnetic responses of SRRs through active probing is possible by means of highly focused beams with the longitudinal magnetic component spatially separated from the transverse electric one.[13–17] The other way around, an SRR on top of a near-field probe passively detects the magnetic component of an electromagnetic wave at optical frequencies.[15,18] The SRR-equipped metal-coated near-field probe nonresonantly couples to the magnetic field component of an electromagnetic wave in a waveguide.[18] Such a probe was employed to detect optical phase variations in the vicinity of a unit cell of a fishnet metamaterial.[15] A metalized SNOM probe without an SRR on top acts as a microscopic conductive ring which produces a magnetic response opposite to the inducing magnetic field. Such a probe can be used to study magnetic light-matter interactions in photonic crystal microcavities.[19,20]

In optics, time-varying currents around subwavelength metallic apertures, plasmon-induced or otherwise, create a variety of effects which attract considerable attention.[21–24] The amplitude of these currents at the tip is conditioned by two effects. The first is the transmission efficiency of modes confined in the dielectric core up to the end of a tapered dielectric waveguide. This efficiency is determined by the lateral dimensions which set the cutoff diameter beyond which only evanescent fields exist. The other effect is guiding of surface plasmon-polaritons (SPPs) on the interior insulator-metal interfaces of a metal-coated SNOM probe, both smooth and corrugated. To the best of our knowledge, propagation of SPPs in such a tapered waveguide generated by internal *arbitrarily* polarized illumination was not considered in the literature except for linear polarization in corrugated SNOM probes.[25,26] However, in tapered stripe waveguides and nanowires it was both theoretically predicted and observed in experiments.[27,28]

Here, in finite difference time-domain (FDTD) simulations in 3D cylindrical coordinates we analyze propagation of azimuthally polarized light through a metal-coated scanning near-field probe and propose radial corrugations to maximize the throughput and energy efficiency of such probes. The properties of the probes are assessed by measuring the transmission efficiency, the characteristics of the focal spot, and energy distribution into the transversal and longitudinal components of the electric and magnetic fields. We also demonstrate, that the energy in the focal spot is predominantly contained within the longitudinal H_z component. As it is shown below, in FDTD simulations we observe a cutoff diameter for modes guided in the tapered dielectric core. However, for plasmon modes a cutoff in the corrugated tapered cylindrical concentrator is not observed for all taper angles considered here.

II. STRUCTURE OF THE MAGNETIC FIELD CONCENTRATOR

According to our multi-quasi-dipole model,[21] that explains the experimental results,[29] charge distribution on the edge of the aperture of an uncorrugated probe is neither uniform nor pointwise. The charge distribution is equivalent to surface plasmons, thus generating them inside a probe increases energy throughput. Corrugations are introduced to ease photon-to-plasmon coupling through momentum matching. SNOM probes with corrugations both along the angular dimension[16] and along the probe length,[25,30] that is axially symmetric, work on the same basic principle. Inverse vectors of groove lattice constants add to momenta of the incident photons to give plasmon wavevectors. In tapered probes of both types plasmons generated at the dielectric-core/metal-coating interface propagate toward the aperture. The difference is that in SNOM probes with axially symmetric grooves, that is along the probe length, the inverse vector of the constant lattice has a relatively narrower distribution than in those corrugated along the angular dimension. For the constant lattice of period Λ the inverse wavevector has a single value $\gamma = 2\pi/\Lambda$. Thus, photons from a narrow spectral range convert into plasmons efficiently. On the contrary, the spectrum of inverse vectors of grooves along the angular dimension is broad, as the lattice constant is linearly proportional to the local radius of the tapered part of the probe. In essence, the inverse vectors are a function of z, $\Gamma(z) = 2\pi/\Lambda(z)$, (see Fig. 1) and contribute to wavevectors of azimuthally polarized broadband illumination resulting in a wide spectrum of efficiently generated plasmons. Due to this fact a magnetic field concentrator can be used for broadband illumination to couple to magnetic resonances of metamaterial elementary cells exhibiting various resonance frequencies. In this way the magnetic concentrator may serve as a probe for a scanning near-field magnetic microscope (SNMM).

Figure 1 presents a schematic illustration of the investigated magnetic field concentrator with corrugations along the angular dimension. The concentrator has a form of a tapered fiber with grooves in the dielectric core that is coated with a continuous layer of aluminum of constant thickness $d = 70$. The dielectric interior of the probe has a refractive index of 1.45, while the aluminum cladding is described by the Drude permittivity model fitted to experimental data obtained by Ordal *et al.*[31] The grooves and metal stripes have a constant azimuthal width of $\pi/8$ yielding a varied grating period suitable for broadband photon-plasmon coupling. The grooves at their deepest are h in depth and gradually become shallower beginning at about three-quarters distance along the side of the cone. Naturally, they cannot be deeper than the radius of the dielectric part of the apex $r = 60$ nm that defines the aperture. In our analysis h varies from 0 to 60 nm. An azimuthally polarized (only E_ϕ present), doughnut-shaped Laguerre-Gauss beam is injected into a dielectric fiber core 4 μm in diameter that is tapered (variable cone angles $\alpha = 40°$, $50°$, $60°$) at the end into a cone. Large taper angles are chosen to limit computer time of the 3D simulations in cylindrical coordinates. The taper angles are, however, experimentally achievable when proper etchant concentration and overlayer liquid are chosen in the Turner method.[32] Moreover, dynamic etching presents an alternative to obtaining large taper angles.[33,34]

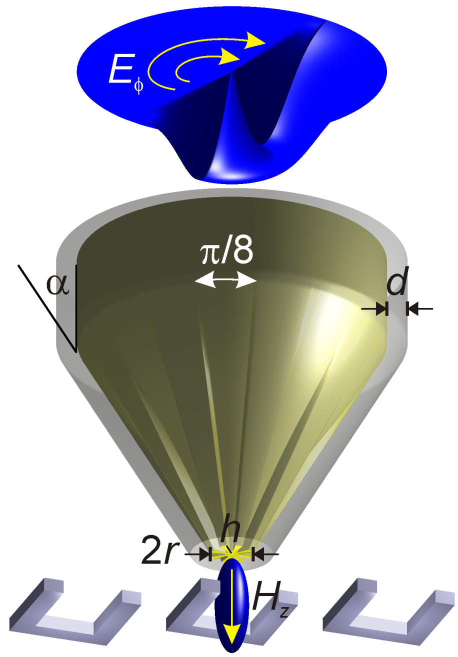

FIG. 1. (color online) Schematic representation of a scanning near-field magnetic probe for generation of a strong longitudinal magnetic field component. A tapered dielectric probe (cone angle α) is corrugated along the angular dimension (groove depth h, azimuthal span $\pi/8$) and covered with a d thick metal layer, the aperture radius is r, including the groove depth. Azimuthally polarized light E_ϕ (cylindrically symmetric Laguerre-Gauss mode) is focused into a focal spot with a dominant longitudinal magnetic field H_z, which is used to excite magnetic moments in metamaterial elements.

III. RESULTS

We begin the analysis by showing a qualitative illustration of the propagation of an electromagnetic wave inside the corrugated SNMM probe in Fig. 2. We focus on the two main field components, *i.e.* the longitudinal magnetic field (Fig. 2a) that is present in the focal spot and the dominant electric component - the azimuthal one (Fig. 2b). The aluminum coating constricts the electromagnetic wave of wavelength $\lambda = 400$ nm to the dielectric core where it propagates until reaching the cutoff. The $h = 60$ nm deep grooves enable the excitation of plasmons that propagate in the grooves beyond the cutoff of the azimuthally polarized beam increasing the transmission efficiency and the intensity of the magnetic field in the focal spot. We use the same color scale in both subfigures to illustrate the energy density for an easy comparison of energy densities of both components. A large

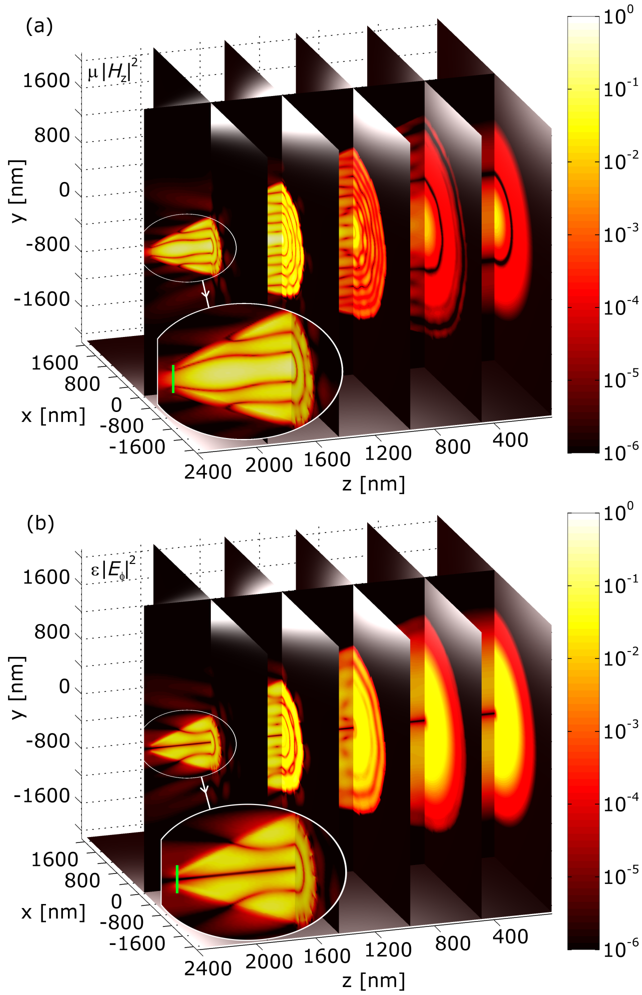

FIG. 2. (color online) Electromagnetic wave propagation inside the investigated probe: (a) longitudinal magnetic energy density ($\mu|H_z|^2$) and (b) azimuthal electric energy density ($\epsilon|E_\phi|^2$). One slice shows the energy density distribution along the direction of propagation (yz-plane), while five slices show transversal xy-plane cross sections. Note the magnified narrow ends of the probe, where the H_z component is maximal at the axis, while the E_ϕ has a minimum. The green lines, 200 nm long, mark the end of the probe. The energy density scale is the same for both components and is logarithmic. The taper angle is 40°, the groove depth is $h = 60$ nm, and wavelength is $\lambda = 400$ nm.

magnetic energy density is seen in the tapered end of the probe and it is much higher (20-fold) than for the incident wave. On the contrary, for E_ϕ the density does not increase beyond the incident value. To make the comparison of the emitted fields easier, we have enlarged the area adjacent to the apex of the probe. The green lines (200 nm long) mark

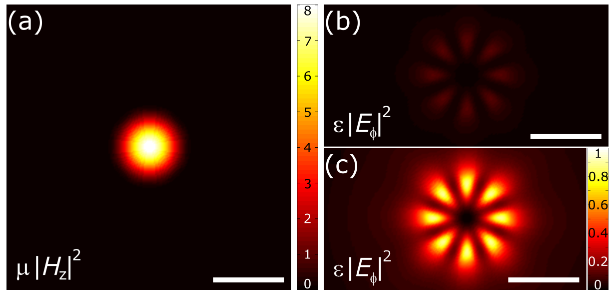

FIG. 3. (color online) Energy density cross sections in focus 10 nm from the aperture plane: (a) shows the magnetic energy density and (b-c) show the same electric energy density. Note, that the scale is the same for (a) and (b) for easy comparison, while the scale in (c) is 8 times lower to show the details of the electric field distribution clearly. The fields are spatially separated with the maximum amplitude of the electric field density more than 8 times lower than the magnetic one and positioned about 20 nm farther away from the axis than the FWHM of the magnetic focal spot. The probe parameters are the same as in Fig. 2: $\alpha = 40°$, $h = 60$ nm, and $\lambda = 400$ nm. The white lines are 100 nm long.

the end of the probe and fields to its left are those radiated from the aperture. This allows for an easy visual comparison of the spatial extent of the H_z and E_ϕ fields, although the logarithmic scale makes the differences in intensities smaller.

The dominant magnetic H_z and electric E_ϕ fields are well separated spatially as shown in Fig. 3. Maximum amplitude of E_ϕ is observed 15–20 nm farther from the propagation axis than the calculated spot size of the magnetic field. Moreover, the amplitude of $\epsilon|E_\phi|^2$ is almost an order of magnitude lower than $\mu|H_z|^2$. Thus, magnetically active structures of lateral dimensions comparable to or smaller than the transversal extent of the magnetic focus will be predominantly excited by the magnetic field.

The quantitative part of our analysis begins with showing the size of the focal spots, defined as the full-width at half-maximum (FWHM) of the magnetic energy density, in Fig. 4a; the computation is carried out 10 nm from the apex of the probes. As expected, sharper probes result in narrower foci. In addition, the presence of grooves decreases the size of the focal spot and this effect is larger for deeper grooves and larger cone angles. Already a relatively shallow 20 nm groove reduces the FWHM by 4 nm, and the deepest by up to 8 nm. This reduction is consistent for the wider taper angles over almost the whole spectral range with only $\alpha = 40°$ behaving slightly differently. Namely, a deviation from this general

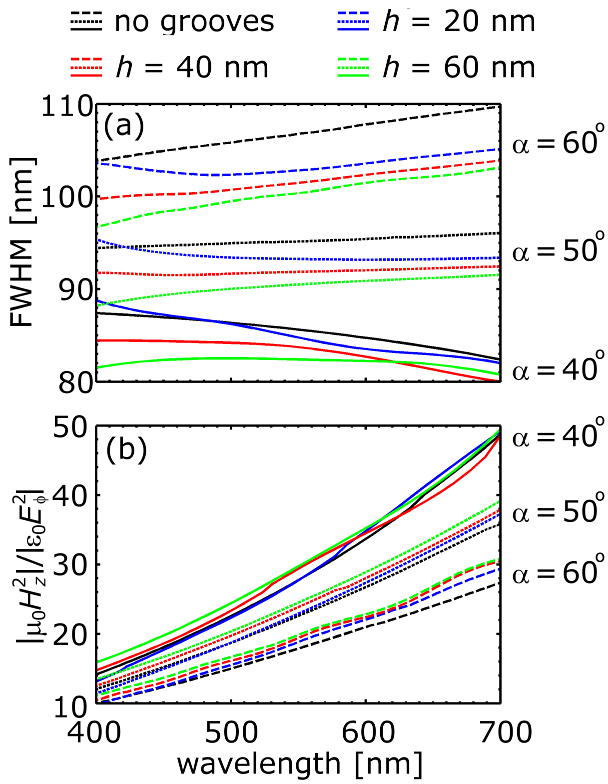

FIG. 4. (color online) Simulation results of magnetic concentrating probes: (a) FWHM and (b) ratio of the magnetic energy to the electric energy in the focal spot for an uncorrugated probe (black) and probes with grooves 20 (blue), 40 (red), and 60 nm (green) deep. The taper angle is 40° for solid lines, 50° dotted lines, an 60° for dashed. Introducing the grooves causes the focal spot diameter to decrease by up to 8 nm and the magnetic-to-electric energy density ratio $\mu_0 H_z^2/\epsilon_0 E_\phi^2$ by a few percent. Note, that both the FWHM and the ratio improve with a decrease of the taper angle. Also, the FWHM is almost constant for $\alpha \approx 50°$, what is beneficial for broadband uniformity of the spot size during measurements.

picture is seen for $h = 20$ nm, as for short wavelengths the FWHM increases slightly.

Figure 4b shows the ratio of magnetic H_z to electric E_ϕ energy density in the focal area. This parameter is important for primarily magnetic coupling to magnetic resonances. As we can see, the ratio, varying from 10 to 50, is much larger than the ratio for a plane wave equal to unity. The ratio increases for smaller taper angles considerably: decreasing α from 60° to 40° shows an 80% jump. For each taper angle the probe with no grooves has the lowest energy ratio and grooves improve this value by up to 10%. In general, the deeper the groove, the better the ratio.

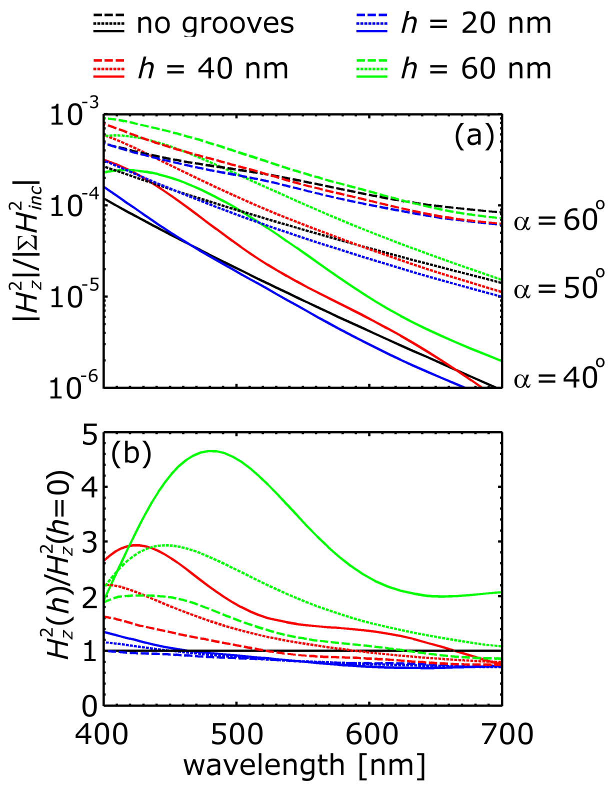

FIG. 5. (color online) Magnetic focal spot formation efficiency: (a) relative to incident power, (b) relative to energy density. (a) A larger taper angle increases the efficiency of magnetic spot formation by one to two orders of magnitude. (b) Grooves increase the efficiency by almost 5-fold and the increase is larger for deeper grooves. The uncorrugated probe is shown in black, probes with grooves 20 nm - blue, 40 nm - red, and 60 nm - green deep. The taper angle is 40° for solid lines, 50° for dotted lines, and 60° for dashed.

As known from previous works, the transmission efficiency of metal-coated near-field probes is quite low.[32] In Fig. 5a we plot it as measured for our probes. It is defined as the energy contained in the longitudinal magnetic field divided by the total incident. Naturally, as the taper angle increases, the energy efficiency gets larger, due to the fact that the distance over which an evanescent solution exists in the probe gets smaller. As this is exponentially dependent on the distance to the aperture, the increase is considerable. Moreover, the cutoff is nearer the apex for shorter wavelengths, so transmission is larger for these wavelengths.

To clearly show the effect of corrugations on the transmission efficiency, we normalize it for each taper angle individually by transmission through an uncorrugated probe $H_z^2(h)/H_z^2(h = 0)$, see Fig. 5b. In this way, in all uncorrugated probes, regardless of the taper angle and

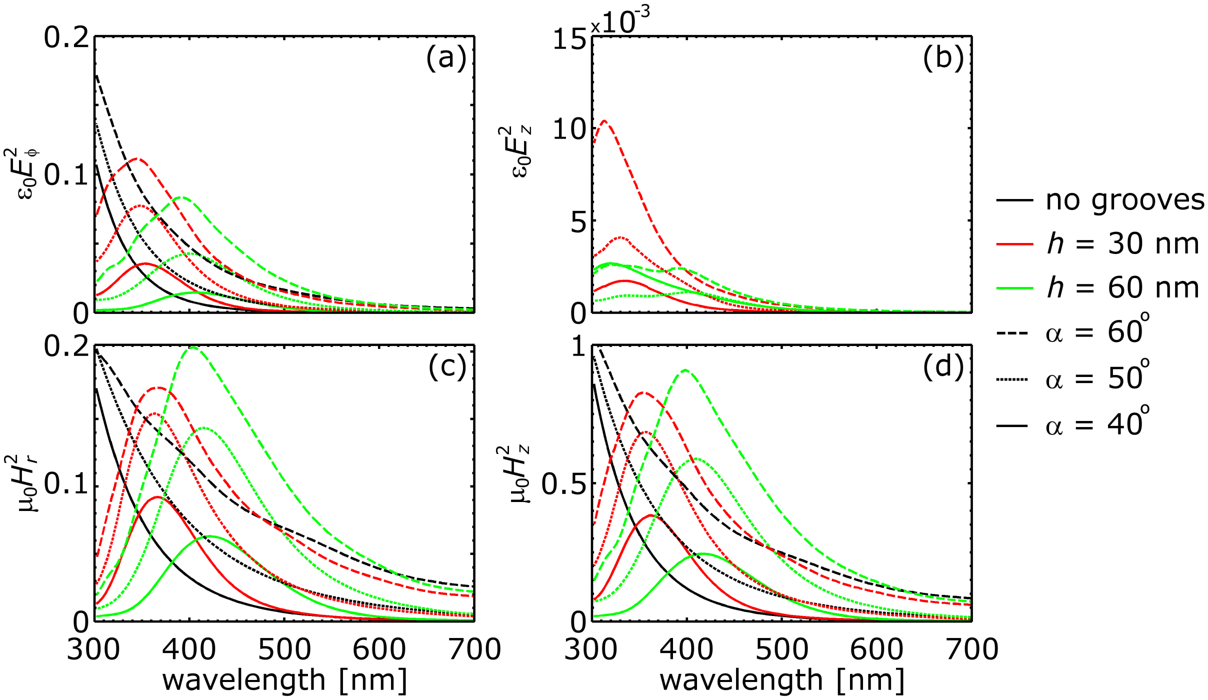

FIG. 6. (color online) Distribution of energy between the dominant components in the focal spot. (a) Azimuthal electric energy density, (b) longitudinal electric energy density, (c) radial magnetic energy density, and (d) longitudinal magnetic energy density. The longitudinal magnetic component carries the dominant part of the energy. The uncorrugated probe is shown in black, probes with 30 nm deep grooves - red, and 60 nm - green. The taper angle is 40° for solid lines, 50° dotted lines, an 60° for dashed.

wavelength, the ratio equals unity. We notice, that the increase of transmission is the largest for $\alpha = 40°$ and $50°$ (solid and dotted lines), as well as for the deepest grooves $h = 60$ nm (green lines). In the best case we predict an enhancement greater than 2 over the whole wavelength range and reaching 5 for blue-green light ($\alpha = 40°$, $h = 60$ nm).

IV. DISCUSSION

The observed results clearly show that metal-coated probes are efficient generators of a longitudinally polarized magnetic field. Moreover, corrugations along the angular dimension combined with azimuthally polarized internal illumination improve the properties of these probes by decreasing the focal spot size, increasing transmission efficiency and the magnetic-to-electric energy densities in the focus.

These three interesting effects are the result of groove-induced excitation of plasmons. Due to boundary conditions, the azimuthal electric field cannot couple to plasmons at the smooth sides of the core, as this would be the forbidden TE mode. However, a grating of grooves along the angular dimension supports plasmons. Moreover, as the radius of the probes shrinks the distance between the grooves decreases and adjacent grooves form a metal-insulator-metal waveguide, which is an efficient channel for propagating plasmons. Naturally, losses play a role, however, the distance over which plasmons need to propagate to reach the aperture is on the order of or smaller than one micron, depending on the taper angle of the probe. Thus, the losses are not very large, and plasmons augment the properties of the investigated probe.

First, we focus on the uncorrugated probe. As it does not support the propagation of surface plasmons, all the observed effects can be understood by looking at propagating and evanescent fields. The probe constricts the electromagnetic fields to the aperture with the electric field amplitude increasing away from the axis. Thus, the apex of the probe can be viewed as an oscillating, circular displacement current with a radius given by the size of the aperture. It is known from electrodynamics, that it generates a strong magnetic field perpendicular to the plane of the current loop.

Now, in the corrugated probe the situation is similar, however, quantitatively changed due to the grooves. In this case the incident field couples to surface plasmons, which propagate along the grooves towards the aperture. The incident field is azimuthally polarized, so both the displacement current between the grooves and the current within the metal grooves are azimuthal. Thus, the above described mechanism of generating the strong longitudinal magnetic field stands. However, plasmons allow for more energy to be transported to the aperture and the amplitude of the azimuthal current is larger than in the uncorrugated probe, what explains the increased energy efficiency of the probe.

Figure 6 presents plots of the four dominant components that contain the most energy inside the focal spot. As can be seen, the longitudinal magnetic component has the most energy, what is consistent with the formation of a H_z focal spot. As we introduce corrugations, large parts of the spectrum are amplified, what is expected from the discussed results. Let us compare the increase of the azimuthal E_ϕ energy (Fig. 6a) and the H_z (Fig. 6d). Concentrating on $\alpha = 60^\circ$ (dashed lines), we notice that when increasing the groove depth from 30 (red) to 60 nm (green), the electric energy decreases (at maximum intensity), while

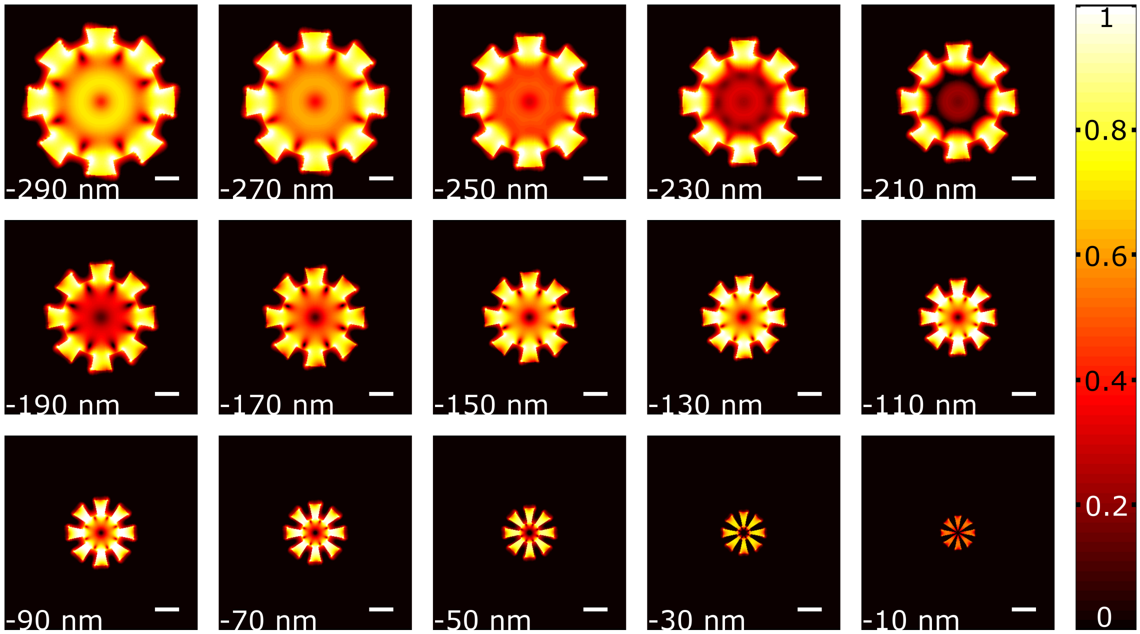

FIG. 7. (color online) Cross sections of electric field amplitude distributions inside a SNMM probe. Starting at the top left corner the distance from subsequent profiles to the aperture decreases by 20 nm. Notice, that the field is confined mostly to the grooves, however, also leaks out of them into the uncorrugated part of the core. Up to -210 nm the incident beam is still seen in the clearance of the core but reaches a cutoff and is stopped. Beyond this location only plasmons and the remaining evanescent field from the incident beam propagate toward the aperture. As the cross section becomes smaller the field intensity increases inside the grooves until about -100 nm, where absorption becomes noticeable. The probe parameters are the same as in Fig. 2: $\alpha = 40°$, $h = 60$ nm, and $\lambda = 400$ nm. The white lines are 100 nm long.

the magnetic energy density increases. For other taper angles both decrease, however, the magnetic energy density decrease is smaller than the electric. Thus, deeper grooves are more efficient than shallow ones at amplifying the magnetic field.

The resonant characteristic of the amplification of field energy is linked to the size of the grooves. The grooves form a periodic metal-insulator waveguide, what is illustrated in Fig. 7 by subsequent cross sections of the probe at various distances from the aperture. An optimum matching of the lateral dimension of the grooves to the frequency of incident light determines efficient guiding. At long wavelengths plasmons are excited relatively far away from the aperture and need to propagate a long distance before they can radiate forming the magnetic focal spot. Decreasing the wavelength pushes the cutoff closer to the aperture and the distance over which plasmons need to propagate to the apex is shorter, reducing at the same time dissipative losses. Thus an increase of field strength is observed as λ decreases. Also, when the mode volume of the plasmons matches the size of the groove the most energy can be transmitted via plasmons. As the wavelength decreases even further the size of the grooved-waveguide becomes too large and plasmons leak out into the dielectric core. There they couple into a wave propagating backward, since propagation in the forward direction is prohibited for modes confined to the dielectric core.

The presence of plasmons also explains the observed reduction of the FWHM. As it is known, a TE-plasmon is forbidden. Thus, the plasmons cannot have maximum amplitude at the metal coating, but away from it, and its radial position depends on the depth of the grooves. Deeper grooves allow plasmons to extend further away from the core-coating interface, so the spot size reduction is larger for deeper grooves.

In Fig. 7, we illustrate plasmon propagation in grooves by showing cross sections of the electric field in the probe. The plots are spaced every 20 nm along the propagation z-axis beginning *ca.* 300 nm from the aperture and ending just before it. It can be seen, that far from the apex a doughnut-like mode confined to the dielectric core can still be identified. It disappears as the diameter of the probe becomes too small and all the remaining energy is guided via the plasmonic modes in the grooves. The energy density inside them undergoes an amplification due to a constriction of the mode volume, however, at the same time dissipation in the metal cladding reduces the amount of guided energy. This balance between the two effects ends about 100 nm from the aperture where the energy density is the greatest. Beyond it plasmons experience dissipative loss, however, at reaching the aperture they still contain more energy than present in the evanescent field of an uncorrugated probe.

V. CONCLUSIONS

Previously described dielectric probes with metal stripes[16] are relatively poor magnetic field concentrators offering in the focal spot only up to 6-fold enhancement of the magnetic-to-electric field energy density ratio. Here, we have shown that metal-coated near-field probes with a smooth dielectric core-metal interface are superior in that they offer magnetic field enhancement values no-lower than 10 and approaching 50. Addition of corrugations along the angular dimension to the metal-coated probes increases the ratio by a further

10% and at the same time decreases the focal spot size and increases energy throughput up to 5 times. Thus, azimuthally corrugated metal-coated probes are efficient generators of a dominant magnetic field component H_z in their focal spot. Moreover, they also have the added benefit of an increased signal-to-noise ratio due to virtually no background that has been stopped by the metal coating.

ACKNOWLEDGMENTS

This work was supported by the Polish National Centre for R&D under the project NR15 0018 06 and the National Science Centre under the projects DEC-2011/01/M/ST3/05734 and DEC-2011/01/B/ST3/02281. The authors are partners in COST Action MP 0803. TJA acknowledges support from the Swedish Foundation for Strategic Research via the metamaterial project SSF RMA08. Simulations were performed in the ICM at the University of Warsaw, grant #G33-7.

REFERENCES

[1] J. Pendry, A. Holden, D. Robins, and W. Stewart, IEEE Trans. Microwave Theory Tech. **47**, 2075 (1999).

[2] D. Smith, W. Padilla, D. Vier, S. Nemat-Nasser, and S. Schultz, Phys. Rev. Lett. **84**, 4184 (2000).

[3] C. Enkrich, F. Pérez-Willard, D. Gerthsen, J. Zhou, T. Koschny, C. M. Soukoulis, M. Wegener, and S. Linden, Adv. Mater. **17**, 2547 (2005).

[4] C. Enkrich, M. Wegener, S. Linden, S. Burger, L. Zschiedrich, F. Schmidt, J. Zhou, T. Koschny, and C. M. Soukoulis, Phys. Rev. Lett. **95**, 203901 (2005).

[5] K. Aydin and E. Ozbay, Opto-Electron. Rev. **14**, 193 (2006).

[6] I. Sersic, M. Frimmer, E. Verhagen, and A. F. Koenderink, Phys. Rev. Lett. **103**, 213902 (2009).

[7] Q. Jiang, X. Y. Zhou, J. Y. Chin, and T. J. Cui, J. Appl. Phys. **110**, 024903 (2011).

[8] Y. Q. Xu, P. H. Zhou, H. B. Zhang, L. Chen, and L. J. Deng, J. Appl. Phys. **110**, 044102 (2011).

[9] T.-Y. Huang, C.-Y. Chen, and T.-J. Yen, J. Appl. Phys. **110**, 093907 (2011).

[10]Y. Jeyaram, S. Jha, M. Agio, J. Loeffler, and Y. Ekinci, Opt. Lett. **35**, 1656 (2010).

[11]R. Merlin, Proc. Natl. Acad. Sci. U.S.A. **106**, 1693 (2009).

[12]E. Devaux, A. Dereux, E. Bourillot, J.-C. Weeber, Y. Lacroute, J.-P. Goudonnet, and C. Girard, Phys. Rev. B **62**, 10504 (2000).

[13]M. Husnik, M. W. Klein, N. Feth, M. Koenig, J. Niegemann, K. Busch, S. Linden, and M. Wegener, Nature Photonics **2**, 614 (2008).

[14]P. Banzer, U. Peschel, S. Quabis, and G. Leuchs, Opt. Express **18**, 10905 (2010).

[15]M. Burresi, D. Diessel, D. van Oosten, S. Linden, M. Wegener, and L. Kuipers, Nano Lett. **10**, 2480 (2010).

[16]T. J. Antosiewicz, P. Wróbel, and T. Szoplik, Opt. Express **18**, 25906 (2010).

[17]J. S. Lee, S. Han, J. Shirdel, S. Koo, D. Sadiq, C. Lienau, , and N. Park, Opt. Express **19**, 12342 (2011).

[18]M. Burresi, D. van Oosten, T. Kampfrath, H. Schoenmaker, R. Heideman, A. Leinse, and L. Kuipers, Science **326**, 550 (2009).

[19]M. Burresi, T. Kampfrath, D. van Oosten, J. Prangsma, B. Song, S. Noda, and L. Kuipers, Phys. Rev. Lett. **105**, 123901 (2010).

[20]S. Vignolini, F. Intonti, F. Riboli, L. Balet, L. Li, M. Francardi, A. Gerardino, A. Fiore, D. Wiersma, and M. Gurioli, Phys. Rev. Lett. **105**, 123902 (2010).

[21]T. J. Antosiewicz and T. Szoplik, Opt. Express **15**, 7845 (2007).

[22]H. W. Kihm, S. M. Koo, Q. H. Kim, K. Bao, J. E. Kihm, W. S. Bak, S. H. Eah, C. Lienau, H. Kim, P. Nordlander, N. J. Halas, N. K. Park, and D.-S. Kim, Nature Commun. **2**, 451 (2011).

[23]I. Sersic, C. Tuambilangana, T. Kampfrath, and A. F. Koenderink, Phys. Rev. B **83**, 245102 (2011).

[24]L. Markley and G. V. Eleftheriades, Metamaterials **5**, 97 (2011).

[25]T. J. Antosiewicz and T. Szoplik, Opt. Express **15**, 10920 (2007).

[26]T. J. Antosiewicz, P. Wróbel, and T. Szoplik, Plasmonics **6**, 11 (2011).

[27]R. Zia, J. A. Schuller, and M. L. Brongersma, Phys. Rev. B **74**, 165415 (2006).

[28]J. Berthelot, F. Tantussi, P. Rai, G. C. des Francs, J.-C. Weeber, A. Dereux, F. Fuso, M. Allegrini, and A. Bouhelier, J. Opt. Soc. Am. B **29**, 226 (2012).

[29]C. Obermüller and K. Karrai, Appl. Phys. Lett. **67**, 3408 (1995).

[30]T. J. Antosiewicz and T. Szoplik, Opto-Electron. Rev. **16**, 451 (2008).

[31]M. Ordal, L. Long, R. Bell, R. Bell, J. R.W. Alexander, and C. Ward, Appl. Opt. **22**, 1099 (1983).

[32]J. Kim and K. Song, Micron **38**, 409 (2007).

[33]H. Muramatsu, K. Homma, N. Chiba, N. Yamamoto, and A. Egawa, J. Mircosc. **194**, 383 (1999).

[34]L. Haber, R. Schaller, J. Johnson, and R. Saykally, J. Microsc. **214**, 27 (2004).